Measurement procedure for acoustic absorption and bulk viscosity of liquids

Leander Claes

Measurement Engineering Group, Paderborn University, Warburger Straße 100, 33098 Paderborn

René Spencer Chatwell

Thermodynamics and Processes Engineering, Technische Universität Berlin, Ernst-Reuter-Platz 1, 10587 Berlin

Elmar Baumhögger

Thermodynamics and Energy Technology, Paderborn University, Warburger Straße 100, 33098 Paderborn

Tim Hetkämper

Measurement Engineering Group, Paderborn University, Warburger Straße 100, 33098 Paderborn

Henning Zeipert

Measurement Engineering Group, Paderborn University, Warburger Straße 100, 33098 Paderborn

Jadran Vrabec

Thermodynamics and Processes Engineering, Technische Universität Berlin, Ernst-Reuter-Platz 1, 10587 Berlin

Bernd Henning

Measurement Engineering Group, Paderborn University, Warburger Straße 100, 33098 Paderborn

Abstract

A measurement procedure using a modified two-chamber pulse-echo experimental setup is presented, enabling acoustic absorption and bulk viscosity (volume viscosity) measurements in liquids up to high temperature and pressure. Acoustic absorption measurements are particularly challenging, since other dissipative effects, such as diffraction at the acoustic source and at acoustic reflectors, are

Email address: claes@emt.uni-paderborn.de (Leander Claes)

typically superimposed to the measurement effect. Acoustic field simulations are performed, allowing to investigate acoustic wave propagation qualitatively. The absorption coefficient is determined by evaluating the signal spectrum's raw moments and applying a method to identify and correct systematic measurement deviations. Measurement uncertainties are estimated by a Monte Carlo method. In order to validate the present measurement procedure, the acoustic absorption in liquid methanol, n-hexane, n-octane, and n-decane is determined experimentally and compared to literature data. The measurement results for methanol are additionally validated by comparison to bulk viscosity data sampled with molecular dynamics simulation.

Keywords: Bulk viscosity, Acoustic absorption

1. Motivation

The analysis and description of fluid dynamic processes are among the most challenging tasks in modern mathematics and engineering. While the fundamental formalism, the Navier-Stokes equations, is well established, its solutions are a matter of ongoing research. For mathematical analysis as well as for application in computational fluid dynamics (*CFD*), the parameters of these equations need to be known. The shear μ_s and bulk viscosity μ_b occur as thermodynamic state properties in the compressible Navier-Stokes equations [1]

$$\rho(\partial_t \mathbf{v} + (\mathbf{v}\cdot\nabla)\mathbf{v}) = -\nabla p + \mu_\mathrm{s}\nabla^2\mathbf{v} + \left(\mu_\mathrm{b} + \frac{\mu_\mathrm{s}}{3}\right)\nabla(\nabla\cdot\mathbf{v})\,, \tag{1}$$

where $\mathbf{v}$, ρ, and p constitute the fluid's hydrodynamic velocity, density, and pressure, respectively. While the shear viscosity is interpretable as a measure of a fluid's linear momentum loss due to shearing motion, the bulk viscosity is a measure of its momentum loss due to compression or dilatation. As evident from equation (1), incompressible fluids ($\nabla\cdot\mathbf{v} = 0$) are not subject to bulk viscosity. For compressible flows, however, the bulk viscosity needs to be known for the specific thermodynamic state of the fluid, requiring an equation of state for the bulk viscosity. A plethora of bulk viscous effects have been observed in compressible fluids, ranging from supersonic flows [2, 3] to shock waves [4, 5, 6, 7]. These investigations, however, suffer from missing, incomplete, or unreliable bulk viscosity data and were consequently restricted to predominantly qualitative results.

A subclass of compressible fluid dynamics problems are acoustic waves. A linearisation of the fluid-mechanical equations for a given pressure and density gives rise to the so-called acoustic approximation, which can predict the propagation and absorption of acoustic waves [8]. Measuring acoustic absorption thus allows the determination of the bulk viscosity for a given thermodynamic state. The absorption of acoustic waves is caused by thermal losses due to heat conduction ν and viscous losses due to shear μ_s and bulk viscosity μ_b. All effects superimpose linearly, yielding the absorption coefficient α for sufficiently small

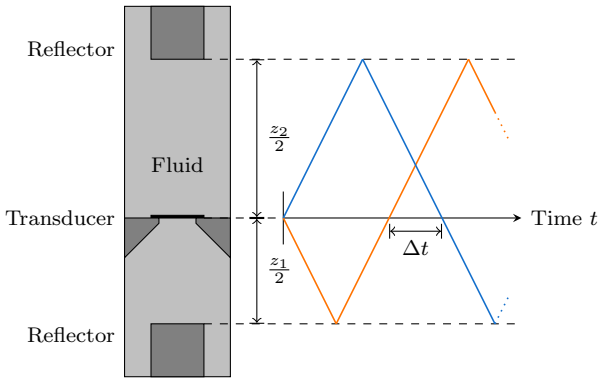

Figure 1: Schematic of the two-chamber pulse-echo measurement setup for sound velocity measurements [10]. A transducer emits sound waves in two differently elongated chambers, which are reflected at the chambers' respective ends. The received signals' time delay is a direct measure of the fluid's thermodynamic sound velocity.

angular frequencies ω [8, 9]

$$\alpha = \frac{\omega^2}{2\rho c^3}\left(\frac{4}{3}\mu_\mathrm{s} + \mu_\mathrm{b} + \frac{c_\mathrm{p} - c_\mathrm{v}}{c_\mathrm{p} \cdot c_\mathrm{v}}\nu\right) , \tag{2}$$

with c, c_p, and c_v being the sound velocity and the specific isobaric and the isochoric heat capacities, respectively. Consequently, determining the bulk viscosity on the basis of acoustic absorption requires a range of thermodynamic properties to be known. In order to lighten notation, the influences of shear viscosity, bulk viscosity, and heat conduction are summarised into the thermo-viscous loss μ_fluid of a respective fluid

$$\mu_\mathrm{fluid} = \frac{4}{3}\mu_\mathrm{s} + \mu_\mathrm{b} + \frac{c_\mathrm{p} - c_\mathrm{v}}{c_\mathrm{p} \cdot c_\mathrm{v}}\nu . \tag{3}$$

Further, the parameter a for quadratically frequency-dependent absorption is introduced

$$a = \frac{\alpha}{\omega^2} = \frac{\mu_\mathrm{fluid}}{2\rho c^3} . \tag{4}$$

In order to measure the sound absorption experimentally, different setups based on the pulse-echo technique exist. Pinkerton [11] uses a single transducer-reflector construction with an adjustable distance. In contrast, Litovitz et al. [12] and Johnson Jr. et al. [13] use a closed cylinder assembly resembling an acoustic waveguide. Available commercial solutions for acoustic absorption measurement are limited to analyses at atmospheric pressure [14]. In the following, a modification of the sound velocity measurement setup by Dubberke et al. [10, 15] is proposed. This setup contains a disc-shaped X-cut quartz transducer (*KVG Quartz Crystal Technology*) with 8 MHz resonance frequency that is mounted openly in order to transmit acoustic signals into two opposing chambers. Two

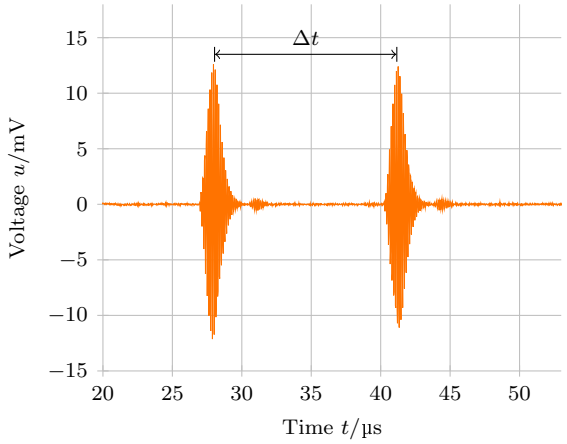

Figure 2: Typical signal as received by the transducer of sound velocity measurements.

acoustic reflectors are positioned so that the acoustic signals travel different distances ($z_1 = 40\,\mathrm{mm}$ and $z_2 = 60\,\mathrm{mm}$) before they are received by the transducer (figure 1). The transducer is driven electrically by a signal generator and the received signals are recorded by an oscilloscope. The signal quality is increased by switching the transducer's electrical connection from the signal generator to the oscilloscope using a purpose-built circuit based on an analogue switch (DG470, *Vishay Siliconix*). While the signals' time delay Δt (figure 2) is a measure of the fluid's sound velocity, the amplitude information can be used to determine acoustic absorption. The measurement cell is housed inside a temperature controlled pressure vessel allowing for measurements at various thermodynamic states, i.e. in the temperature range between 220 K and 480 K up to a pressure of 100 MPa. This setup is a starting point for the design of a measurement procedure for acoustic absorption. In contrast to previous approaches [11, 16, 13], this experimental setup does not rely on movable reflectors. Signal processing based on properties of the measurement signals' spectra is used to determine the parameters of frequency-dependent absorption mechanisms directly. Expected systematic measurement deviations are reduced by targeted modifications of the experimental setup. Residual deviations are identified using reference measurements and corrected accordingly.

2. Signal processing

Signal attenuation can experimentally be determined by comparing the peak values $\hat{u}(z_1)$ and $\hat{u}(z_2)$ of the signal at different spatial positions z_1 and z_2. It is common practice to anticipate an exponential decay of a wave's amplitude, resulting in the classical expression for acoustic absorption α

$$\alpha = \frac{1}{z_2 - z_1} \ln\left(\frac{\hat{u}(z_1)}{\hat{u}(z_2)}\right) . \tag{5}$$

Evaluating the bulk viscosity by comparing equations (3) and (5) requires the acoustic signal's angular frequency ω to be known. The signal's mean frequency can be used as an estimate for ω, but this would cause systematic deviations arising primarily from strong absorption and large signal bandwidths [17, p. 173]. Alternatively, the properties of the signal spectra can be evaluated by determining the parameter a of a quadratically frequency-dependent absorption model $\alpha = a\omega^2$. In the following, two methods are presented. While the first is based on changes of the centre frequency, the second is formulated in terms of the raw moments of the signal spectra.

The frequency dependence of the absorption mechanism affects the acoustic signal's various frequencies differently, i.e. the higher frequency components are absorbed stronger than the signal's lower frequency components, thus giving rise to dispersion. Consequently, the effect on the signals amplitude spectrum $U(\omega, z)$ at any given distance from the transducer $z \geq 0$ can be described by

$$U(\omega, z) = U_0(\omega)\mathrm{e}^{-\alpha z} = U_0(\omega)\mathrm{e}^{-a\omega^2 z} \,, \tag{6}$$

with $U_0(\omega)$ being the amplitude spectrum of the signal emitted by the transducer. This approach is similar to the methods introduced by Fink et al. [18] and Quan et al. [19], who estimate the acoustic signal attenuation by the centre frequency shift. The signal spectrum $U_0(\omega)$ can be chosen arbitrarily and hence can also account for the transducer's frequency response as well as the electrical transmission by assuming linearity and time-independence during signal acquisition without altering any results. This is particularly necessary because the transducer used shows pronounced resonant behaviour and thus strongly frequency-dependent transmission characteristics. The signal spectrum's i-th raw moment m_i can thus be formulated as

$$m_i(z) = \int_{-\infty}^{\infty} \omega^i \cdot U(\omega, z)\mathrm{d}\,\omega \tag{7}$$

$$= \int_{-\infty}^{\infty} \omega^i \cdot U_0(\omega)\mathrm{e}^{-a\omega^2 z}\mathrm{d}\,\omega \,, \tag{8}$$

and its changes are assessed by taking the spatial derivative

$$\partial_z m_i(z) = -a \int_{-\infty}^{\infty} \omega^{i+2} \cdot U_0(\omega)\mathrm{e}^{-a\omega^2 z}\mathrm{d}\,\omega \,. \tag{9}$$

A comparison between equations (8) and (9) discloses the integral (9) to be the spectrum's $(i+2)$-th raw moment, leading to the following relation

$$\partial_z m_i(z) = -a \cdot m_{i+2}(z) \,. \tag{10}$$

The centre frequency ω_c of a signal can be expressed as a quotient of raw moments [18, 19]

$$\omega_\mathrm{c} = \frac{m_1(z)}{m_0(z)} \,. \tag{11}$$

Applying the quotient rule and exploiting equation (10) yields the following expression for the spatial derivative of the centre frequency

$$\partial_z \omega_\mathrm{c} = a\frac{m_2(z)m_1(z) - m_3(z)m_0(z)}{m_0^2(z)} \,. \tag{12}$$

The absorption parameter a can thus be determined if the raw moments and the change in the centre frequency are known

$$a = \partial_z(\omega_\mathrm{c}) \frac{m_0^2(z)}{m_2(z)m_1(z) - m_3(z)m_0(z)} \,. \tag{13}$$

While raw moments of a signal's amplitude spectrum can be determined numerically, the centre frequency's derivative needs to be estimated. As an almost linear decay of the centre frequency is expected [20], finite differences of the centre frequency of the signals at z_1 and z_2 are applied. For an application to measurement signals, z can be chosen arbitrarily.

In an alternative approach for the estimation of the absorption parameter a, equation (10) can be evaluated directly

$$a = -\frac{\partial_z m_i(z)}{m_{i+2}(z)} \,. \tag{14}$$

The raw moments of a signal's amplitude spectrum can be determined numerically. The moment's derivative, however, has to be estimated. While the intuitive approach would again be to apply finite differences, a different approximation leads to more conclusive results and takes the nature of absorption into account. It can be shown that for signals with sufficiently limited bandwidth, raw moments of the spectrum show an exponential decay [17, p. 167 ff.]. Thus, an exponential expression

$$m_i(z) = A_i \mathrm{e}^{\,B_i z} \tag{15}$$

for $m_i(z)$ can be identified and derived analytically. Inserting the resulting expression into equation (14), while arbitrarily choosing $i = 0$, yields an estimator for the absorption parameter depending exclusively on the signals' raw moments

$$a = \frac{1}{z_2 - z_1} \frac{m_0(z_1)}{m_2(z_1)} \ln\left(\frac{m_0(z_1)}{m_0(z_2)}\right) \,, \tag{16}$$

which bears some resemblance with the monochromatic approach of equation (5). This new approach, however, directly yields the parameter a of a quadratically frequency-dependent absorption model by exploiting the dispersive nature of the absorption mechanism. Further, the result is not influenced by the frequency-dependent transmission properties of the transducer, which are due to its resonant characteristics and may change between measurements. No assumptions are made about the amplitude spectrum $U_0(\omega)$ transmitted by the transducer other than that it has a limited bandwidth. The approach can also be adapted to quantify absorption of arbitrary wave-like phenomena obeying other power laws and can be expanded to estimate the parameters of absorption models with multiple parameters [21].

In order to arrive at a robust absorption estimation method, its stability with respect to noise and other interfering effects has to be established first. Consequently, both methods are applied to measurements signals of liquid methanol, obtained from the original measurement setup. The dataset explicitly contains

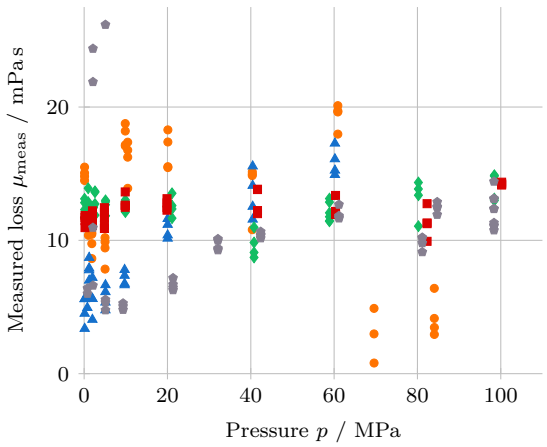

Figure 3: Thermo-viscous loss measured experimentally using the centre frequency shift approach (equation (13)) for methanol at various temperatures (● 221 K, ▲ 244 K, ♦ 300 K, ■ 350 K, and ⬟ 400 K) as a function of pressure.

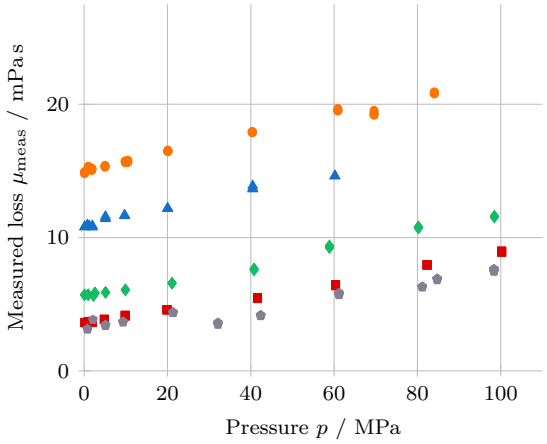

Figure 4: Thermo-viscous loss measured experimentally using the raw moment approach (equation (16)) for methanol at various temperatures (● 221 K, ▲ 244 K, ♦ 300 K, ■ 350 K, and ⬟ 400 K) as a function of pressure.

repeated measurements at each state point that should ideally yield the same result. The centre frequency shift approach does not yield a clear relation between the measured thermo-viscous loss μ_{meas} and the thermodynamic state of the fluid, cf. figure 3. Repeated measurements even show large variations. This instability is attributed to the small relative shift of the signals' centre frequency, which could be as low as 0.1 %. In contrast, evaluating the raw moments of the signal spectra yields significantly less variation among repeated measurements, cf. figure 4, and indicates a clear relation between the measured thermo-viscous loss μ_{meas} and the thermodynamic state. Consequently, evaluating the raw moments of the signal spectra is the preferred method to determine the absorption parameter a. However, the values given in figure 4 are still superimposed by parasitic effects which have to be analysed and corrected.

3. Analysis of systematic measurement deviations

In contrast to the effects of the transducer's frequency response and the electrical signal transmission that can be accounted for by the methods presented above, systematic measurement deviations caused by diffraction and imperfect reflections need to be corrected with other approaches. The approach presented here is based on literature data for bulk viscosity and acoustic absorption as a reference to derive a correcting procedure using a number of reference measurements. A prerequisite for the proposed procedure is, however, that the deviations are deterministic and continuous such that they can be described with elementary mathematical expressions.

The expected systematic measurement deviations are caused by wave propagation and should therefore only depend on acoustic properties, such as the sound velocity c, density ρ, and thermo-viscous loss μ_{fluid}. A simulation model of the measurement setup is created allowing to investigate the systematic measurement deviations qualitatively. This virtual model facilitates a full variation of the fluid properties c, ρ, and μ_{fluid}. The field equations are solved numerically by finite differences in time domain (FDTD) using a dedicated simulation tool [22]. The wavelengths of the simulated acoustic waves are small compared to the overall size of the simulation domain so that a rather fine grid resolution of around $1.2 \cdot 10^7$ spatial points is required. Despite reducing the computational effort by exploiting the setup's axial symmetry, a simulation run takes approximately 50 h on current hardware (Xeon E5-2670, *Intel*). Each run yields a time signal that leads to the absorption parameter a_{sim} by applying the raw moments method. Two distinct simulation studies are conducted and their results are discussed on the basis of the simulated thermo-viscous loss $\mu_{\mathrm{sim}} = 2a_{\mathrm{sim}}\rho c^3$.

In a first simulation series, the original setup is virtually replicated (figure 1). The transducer mounting is included, covering the outer ring of one side of the transducer's active area. Consequently, the transmission characteristics and the transducer's sensitivity for incident acoustic waves are expected to differ for each side. If there were no interfering effects, the thermo-viscous loss determined by evaluating the simulated signals μ_{sim} would be equal to the thermo-viscous loss in the fluid μ_{fluid}. The results depicted in figure 5, however, show significant

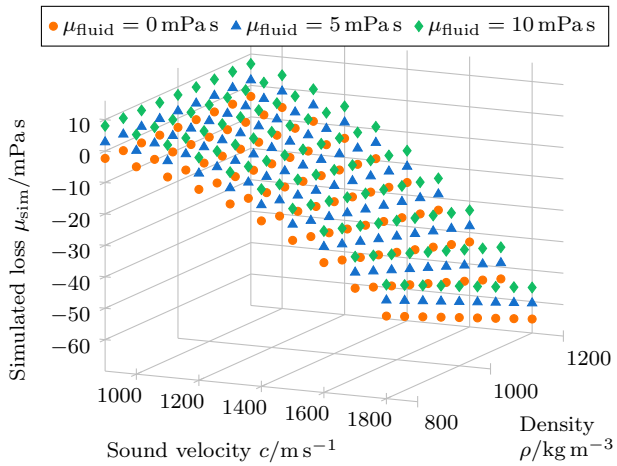

Figure 5: Thermo-viscous loss μ_{sim} determined from simulation for asymmetric emission characteristics, i.e. including the transducer mounting, for varying fluid parameters. The simulation results clearly indicate large systematic deviations.

deviations from the ideal values. While the deviations appear continuous with respect to the fluid parameters, the most notable feature is that the determined values for μ_{meas} are partially negative. This effect is also observable in the time domain, as signals having propagated through the longer chamber seem less attenuated than signals that propagated through the shorter chamber. This anomaly is explained in light of the asymmetric transducer mounting, giving rise to an apparent absorption of the waves inciting from the shorter chamber and consequently yielding negative values for μ_{sim} at some thermodynamic states. A similar effect is observed in the original setup [10], but proves to be inconsequential for sound velocity measurements.

A second simulation series is conducted without accounting for effects caused by the transducer mounting. In this case, the results (figure 6) show a significantly lower deviation from the ideal values, which is positive for all examined combinations of fluid parameter values. The deviation is again continuous and increases with sound velocity and density. Furthermore, the observed systematic deviations seem to superimpose to the fluid's proper thermo-viscous loss additively

$$\mu_{\text{sim}} \approx \mu_{\text{fluid}} + \mu_{\text{dev}} \,. \tag{17}$$

The same can be observed for the simulations which account for the effects of the asymmetric transducer mounting (figure 5). The additive superposition is, however, less noticeable due to the large systematic deviations. This fact can be exploited to develop a method to correct the deviation, which is described in section 5. Additionally, a modification of the experimental setup is proposed aiming to reduce the parasitic effects on the measured thermo-viscous loss μ_{meas} by creating symmetrical emission characteristics.

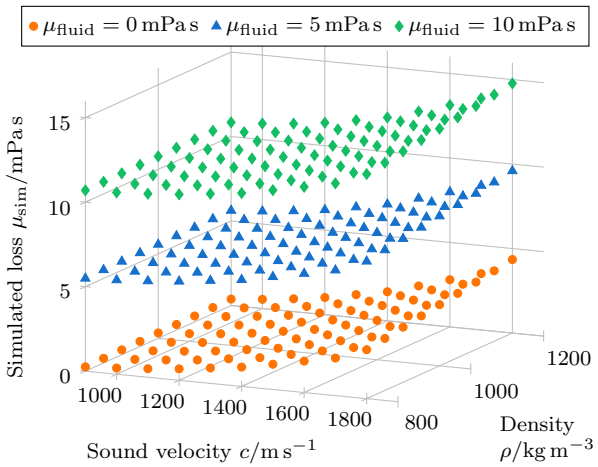

Figure 6: Thermo-viscous loss μ_{sim} determined from simulation for symmetric emission characteristics, i.e. neglecting the transducer mounting, for varying fluid parameters. The simulation results indicate increasing deviations for higher density and sound velocity.

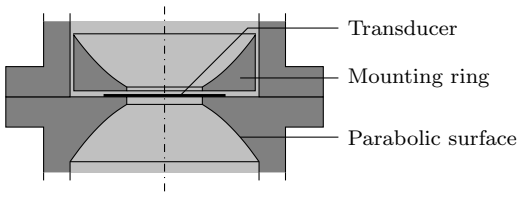

Figure 7: Schematic of the transducer mounting to enable symmetrical emission of acoustic waves in both directions.

4. Modification of the measurement setup

On the basis of the present simulation results, a modification of the two-chamber pulse-echo measurement setup is proposed, aiming to reduce the systematic measurement deviation. The original setup (figure 1) aims at for precision measurements of the sound velocity of liquids. It is designed with a single-sided, conically shaped transducer mounting, having a circular opening facing the longer chamber and thus giving rise to asymmetric emission characteristics. The quartz crystal is placed on the opening, fixed and electrically connected with spring elements [10].

This mounting geometry is revised to facilitate symmetric emission characteristics. Special care is taken as the mounting is also required to connect the transducer electrically, while avoiding materials that may be unsuited for high temperature and pressure environments. Symmetry is achieved by constructing a conically shaped mounting ring that partially shields the transducer from the longer chamber in accordance with the partial shielding of the opposing structure facing the shorter chamber, cf. figure 7. The mounting ring is positioned

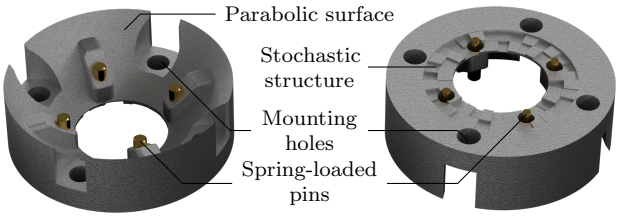

Figure 8: Upper and lower view of the model for the mounting ring with spring-loaded pins inserted.

slightly above the transducer, since the ring serves as an electric contact for the upper electrode and has to be insulated from other components that are contact in with the lower electrode. This gap between the ring and the transducer also protects the latter from mechanical damage.

The gap between transducer and the mounting ring, although necessary, entails unwanted reverberations and resonance effects when the transducer emits acoustic waves. In an effort to suppress these unwanted effects, a stochastic structure is designed [23], i.e. prismatic elements with randomized heights are created at the ring's lower surface, causing diffuse reflections. Previous sound velocity measurements indicated the existence of structure-borne sound in the transducer mounting, as evident from additional echoes in time domain. Thus parabolic surfaces are favoured over straight ones to divert these signals away from the transducer.

The highly detailed and finely structured parts have to sustain high temperatures and are consequently manufactured additively from stainless steel (1.4550) by selective laser melting. Spring-loaded pins (F708, *FEINMETALL*) are used to electrically connect the upper electrode to the mounting ring, cf. figure 8. The simplified geometry of the mounting ring (figure 7) needs to be modified to accommodate for these pins, requiring housings that protrude from the parabolic surface (figure 8). A disc-shaped X-cut quartz crystal (*KVG Quartz Crystal Technology*) with a resonance frequency of 8 MHz is used as transducer. The electrodes on the quartz crystal are in a so-called 'keyhole' configuration that requires opposing spring-loaded pins for a good electrical contact. For improved stability, two additional pins are used. The mounting ring is fixed to the structure by screw holes leaving space for polytetrafluoroethylene washers ensuring proper electrical insulation. For symmetry reasons, four mounting holes are realised along with space for the washers (figure 8). In an effort to ensure the transducer's surroundings to be as symmetric as possible, the pin housings are mirrored on the structure's opposing site. As no spring-loaded pins are required to contact the lower electrode, the housings are instead used to accommodate the screws, which hold the ring element in place.

A sectional view of the modified setup is presented in figure 9, showing the 20 mm and 30 mm spacers used to realise the shorter and longer sound propagation chambers, respectively. While both spacers are made from stainless steel,

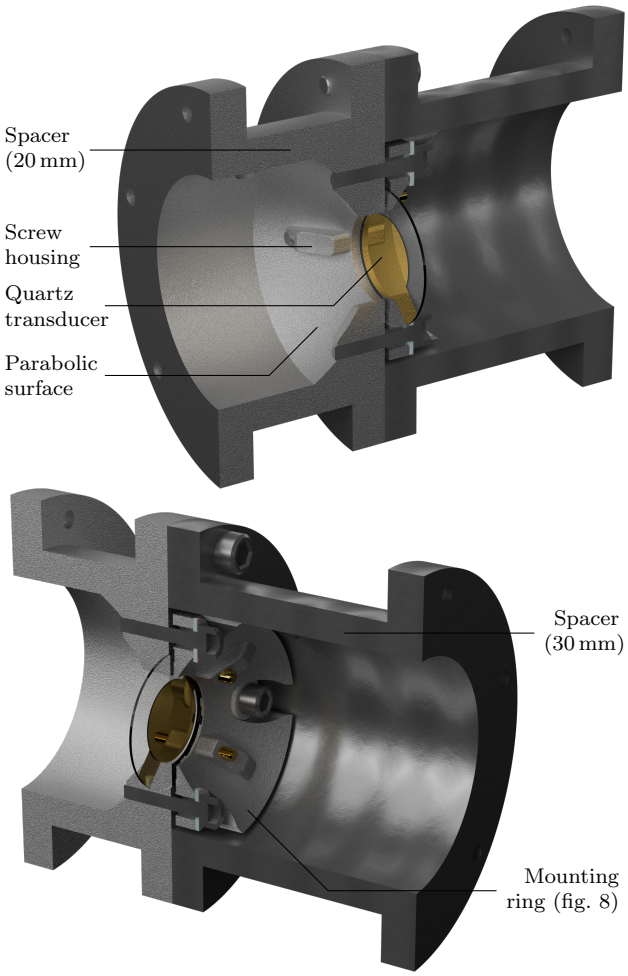

Figure 9: Sectional view of the transducer mounting for symmetrical radiation from the direction of the parabolic lower element (top) and the inserted mounting ring (bottom).

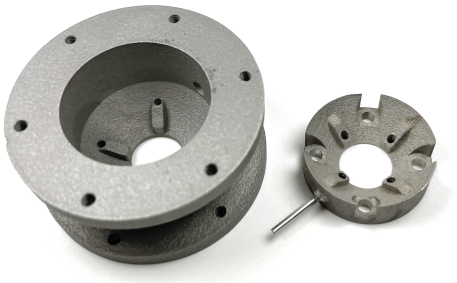

Figure 10: Additively manufactured 20 mm spacer (left) and ring element (right) with wire for electrical contact.

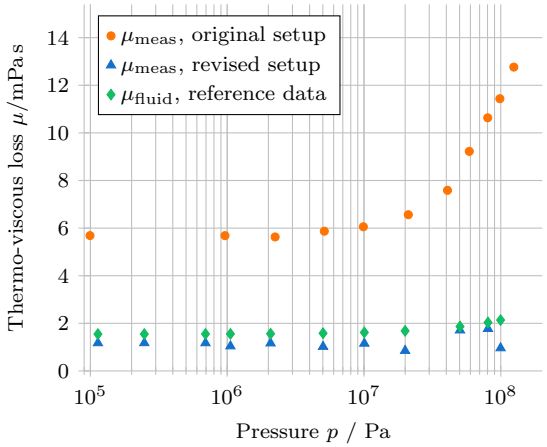

Figure 11: Measured thermo-viscous loss μ_{meas} of liquid methanol at constant temperature 300 K and varying pressure obtained with the original and revised setup, compared to interpolated literature data [24, 25].

the shorter spacer is manufactured additively and the longer spacer is made by spin forming due to its nearly axisymmetric geometry. Both additively manufactured parts, the short spacer and the ring element, are shown in figure 10. The transducer's excitation signal is supplied through a wire brazed to the mounting ring and the rest of the setup is kept at ground potential. Completing the measurement cell, the acoustic reflectors are attached using screws to the spacers through six circumferential threads at each spacer's respective end. This approach is adapted from the original setup [10], allowing for a quick access to different elements. As in the original setup (cf. section 1), the transducer is driven by a sinusoidal burst supplied by a signal generator and the signals are recorded using an oscilloscope. The revised setup is placed in a temperature controlled pressure vessel similar to the original setup allowing measurements at defined thermodynamic states [15].

To evaluate the improvements and demonstrate the reduction of the systematic measurement deviation, the acoustic absorption in liquid methanol is determined at various thermodynamic states. A comparison of the measured thermo-viscous loss μ_{meas} obtained by the original setup and the revised setup with interpolated literature data [24, 25] is given in figure 11. While the thermo-viscous loss μ_{meas} measured with the original setup shows large deviations that tend to increase with rising pressure, the revised setup shows significantly reduced systematic deviations that are less dependent on pressure. However, the results of the revised setup show some scattering.

5. Correction procedure for systematic measurement deviations

The simulation study in section 3 shows that the systematic measurement deviation due to the acoustic wave propagation in the measurement system is

expected to be continuous and dependent on the properties of the fluid. Further, the deviation appears to be additively superimposed to the loss in the fluid. However, as the simulation model does not account for all effects that occur in the physical measurement setup, the results of the simulations cannot directly be used to correct the systematic measurement deviation that remains after modifying the setup (figure 11). While a correction can be found by identifying a polynomial expression of the sound velocity c, the density ρ, and the measured thermo-viscous loss μ_{meas} [26], qualitative aspects of the simulation results can be exploited for a more robust approach. A reliable method for parametrising and identifying the systematic measurement deviation is advantageous, as disassembly of the setup, which is required to remove contaminations (e.g. particles from valve wear), typically changes its acoustic properties and thus necessitates repeating the procedure. Inspired by the simulation results in section 3, the proposed correction procedure presupposes these effects to superimpose to the fluid's proper thermo-viscous loss additively. Then they can be formulated by some function $P(c, \rho)$ of sound velocity and density

$$\mu_{\mathrm{fluid}} \approx \mu_{\mathrm{meas}} - P(c, \rho) \; . \tag{18}$$

A close examination of the simulation results indicates a small factor (close to unity) between the simulated and the fluid's proper thermo-viscous loss that is best observed at moderate sound velocity $c = 900\,\mathrm{m\,s^{-1}}$ and density $\rho = 800\,\mathrm{kg\,m^{-3}}$, cf. figure 6. A progressively rising offset between the fluid's proper thermo-viscous loss μ_{fluid} and the simulated result μ_{sim} is visible. This factor is accounted for by an additional fitting parameter b_μ

$$\mu_{\mathrm{fluid}} = b_\mu \mu_{\mathrm{meas}} - P(c, \rho) \; , \tag{19}$$

which is considered to be close to unity for a physically sound approach. The contributions of the systematic measurement deviation $P(c, \rho)$ are further assumed to be polynomial functions

$$P(c, \rho) = \sum_{i,m,n} b_i c^m \rho^n \; , \; m, n \in [0, N] \; , \tag{20}$$

whose order $N \leq 3$ is restricted since the number of possible combinations increases with rising polynomial order. The number $N_{b_i} \leq 5$ of non-zero coefficients b_i restricted as well. How many coefficients are non-zero depends on how successful the efforts to create symmetrical characteristics described in section 4 are, as indicated by a comparison between figures 5 and 6. The requirement that the additional coefficient b_μ has to be close to unity can be utilised in order to find a suitable parametrisation for $P(c, \rho)$.

The present correction relies on accurate reference data for the bulk viscosity and is demonstrated using liquid methanol and n-hexane as reference fluids. Recalling equation (3), the individual contributions to the fluid's proper thermo-viscous loss superimpose linearly, with the respective shear viscosity [27, 28], thermal conductivity [29, 30] and heat capacities [31, 32] that are determined

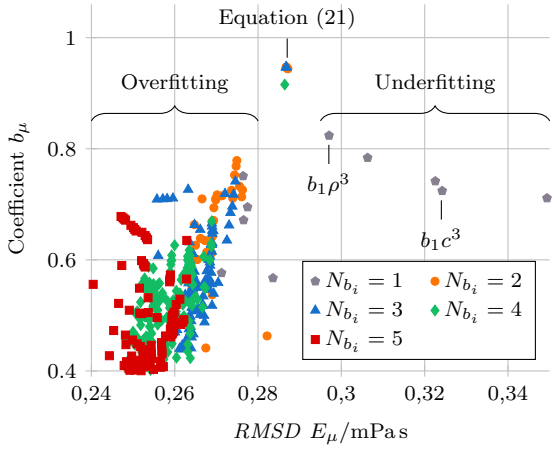

Figure 12: Values of the coefficient b_μ and *RMSD* E_μ for different variants of $P(c, \rho)$ with different numbers of coefficients N_{b_i}.

with the most recent equations of state. If lesser known fluids are to be analysed, the sound velocity may also be determined by evaluating the delay of the measurement signals. In contrast, the bulk viscosity reference data are determined by interpolating selected literature data [33, 24, 25, 34, 35]. Using these data, reference measurements are conducted at 15 different thermodynamic states for methanol and at 11 different thermodynamic states for n-hexane. The subsequently performed acoustic absorption measurements of methanol and n-hexane with the revised setup yield the measured thermo-viscous loss $\mu_{\text{mess}} = 2a_{\text{mess}}\rho c^3$.

The following procedure is proposed to find a suitable expression for $P(c, \rho)$ using the reference measurement data. The least-squares fit of equation (19) for all variants of the polynomial $P(c, \rho)$ is determined, identifying the values for b_μ as well as for the coefficients b_i. A variant of $P(c, \rho)$ is selected, which shows b_μ close to unity, small root-mean-square deviation (*RMSD*) E_μ, and as few coefficients N_{b_i} as possible. Only few variants of $P(c, \rho)$ are identified with $b_\mu \approx 1$ (figure 12). There are several variants, typically with a large numbers of coefficients N_{b_i}, that will fit the reference data better, resulting in a lower *RMSD*. However, b_μ is also low, indicating overfitting. There are also some variations with low b_μ, but a rather high *RMSD* and as few as one coefficient that indicate underfitting. Of the variants that show $b_\mu \approx 1$, a second-order polynomial with *RMSD* $E_\mu = 0.287\,\text{mPa s}$

$$\mu_{\text{fluid}} = b_\mu \mu_{\text{mess}} - (b_1 \cdot \rho^2 + b_2 \cdot \rho)\,, \tag{21}$$

and two parameters b_i with values disclosed in table 1 is selected. The selected polynomial equation (21) does not depend explicitly on the sound velocity, although the simulation results (section 3) imply that the dependence on the sound velocity exceeds the dependence on density. However, realisations of $P(c, \rho)$ that are close to equation (21) in figure 12 do depend on sound velocity.

Table 1: Results for the coefficients of equation (21).

b_μ	b_1	b_2
0.9472	$-4.5429 \cdot 10^{-9}$	$2.8507 \cdot 10^{-6}$
1	$\mathrm{Pa\,s\,m^6\,kg^{-2}}$	$\mathrm{Pa\,s\,m^3\,kg^{-1}}$

As the deviation to be corrected appears to be approximately constant with respect to the properties of the fluid (cf. figure 11), this almost constant term can be expressed in several ways that yield similar numerical results. Conversely, applying the method to previously recorded data from the original setup indicates a strong dependence on sound velocity, yielding the following expression [17, p. 111]:

$$\mu_{\mathrm{fluid}} = b_\mu \mu_{\mathrm{meas}} - (b_1 \cdot c\rho^2 + b_2 \cdot c\rho + b_3 \cdot c^2 + b_4 \cdot c) \; . \tag{22}$$

The correction (equation (21)) is parametrised and identified based on reference data. Applying it to other measurement data is thus only possible if the acoustic behaviour of the fluid to be analysed is similar to that of the reference fluids. The actual measurement range is quantified by identifying a convex hull [36] enveloping the reference data's thermodynamic states in the sound velocity-density plane. As the deviation is expected to be continuous, equation (21) is expected to be valid in the vicinity of the reference measurements. Thus, the validity of the correction is expanded by including measurement data sets that have a relative deviation of less than 2 % with respect to sound velocity and density. This range is depicted in figure 13 along with additional data sets for methanol and n-hexane that are not included in the reference data set, as well as n-octane and n-decane.

Finally, an uncertainty analysis on the basis of a Monte Carlo method [37, 38] is performed. Uncertainties for the principal measurements (temperature and pressure measurement as well as the uncertainties of the oscilloscope's time base and voltage measurement) are taken into account as type B uncertainties and propagated through all computational steps. Further, the uncertainties specified by the respective equations of state for all required thermodynamic properties (sound velocity, density, shear viscosity, thermal conductivity, and the specific heat capacities) are considered similarly. Of particular interest are the uncertainties u_{corr} caused by the correction method, which are estimated according to [39]

$$u_{\mathrm{corr}}^2 = \frac{1}{M - (N_{b_i} + 1)} \sum_{n=1}^{M} \left(\mu_{\mathrm{ref},n} - \mu_{\mathrm{fluid},n}\right)^2 \; , \tag{23}$$

considering the $M = 26$ supporting reference data points, while $N_{b_i} + 1$ is the number of parameters of the correction that need to be identified (the one additional parameter is b_μ). If the term $N_{b_i} + 1$ is dropped, the expression would

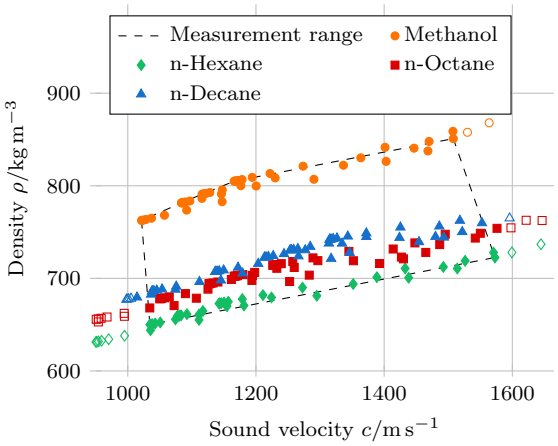

Figure 13: Measurement range as defined by a convex hull enveloping the reference measurements in the sound velocity-density plane. Valid (●) and invalid (○) data sets based on a tolerance of 2 % relative deviation.

be identical to the *RMSD* of the fit. It is apparent that for a larger number of parameters N_{b_i}, the uncertainty contributed by the correction increases, providing another reason for a small number of parameters. The uncertainties of the employed reference data from the literature need to be approximated, as most publications predate the introduction of the concept of measurement uncertainty. Some authors specify repeat measurement accuracies [33, 35] of around or below 5 %, a value that is assumed as additive type B uncertainty with uniform distribution. The resulting standard uncertainties for each measurement value are shown along with the results in the following section (figures 14 to 16).

6. Results and discussion

The proposed modifications of the two-chamber pulse-echo measurement setup significantly reduce the systematic measurement deviation of acoustic absorption measurements. The subsequently applied signal processing in combination with the correction accounts for the remaining deviations between the measured loss μ_{meas} and the proper thermo-viscous loss μ_{fluid}.

However, verification is only partially possible, as values for the measured quantities for some of the fluids have not been published before. Thus, to check for plausibility, the results for fluids of the homologous series of n-alkanes are evaluated. As earlier publications for primary alcohols show that thermo-viscous loss μ_{fluid} and the bulk viscosity μ_{b} increase with molecular size [16], the same is expected for the n-alkanes, but has, as of now, not been experimentally investigated.

The experimental results for the n-alkanes at constant temperature 303 K and varying pressure corroborate the anticipated increase of μ_{meas} with molecular size, cf. figure 14. Further, they indicate the measured thermo-viscous loss

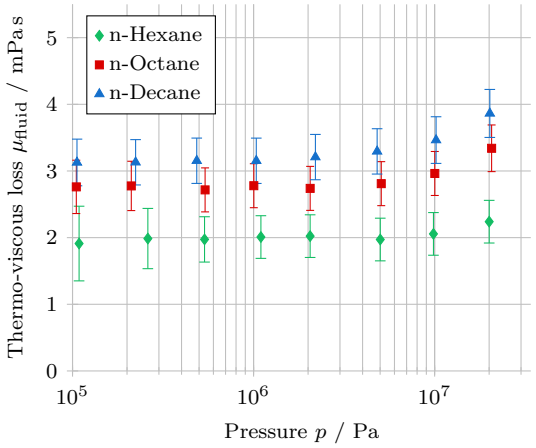

Figure 14: Experimentally determined thermo-viscous loss μ_{fluid} of n-hexane, n-octane, and n-decane with its respective standard uncertainties at constant temperature 303 K and varying pressure.

to increase with rising pressure, a behaviour that has already been observed for aliphatic carbon hydrates [33].

Following equation (2), the computation of a substance's bulk viscosity from μ_{meas} requires a range of its thermodynamic properties to be known, i.e. thermal conductivity ν, specific heat capacities c_{p}, c_{v}, and shear viscosity μ_{s}, which for the investigated fluids are taken from the literature [27, 28, 40, 29, 30, 41, 31, 32, 42]. The bulk viscosity follows the same trend as μ_{meas}, cf. figure 15, i.e. it increases with rising molecular size and pressure, thus matching previous observations for toluene and methanol [33, 25].

The relatively large uncertainties can be traced to the correction procedure and the *RMSD* of 0.287 mPa s, which is very close to the observed uncertainty of each measurement. As the absolute uncertainties do not change significantly with the values of the measured quantity, this also implies that measurements performed on fluids with a large thermo-viscous loss will show a small relative uncertainty. This is plausible as the measurement effect increases with the measurement quantity in this absorption measurement procedure variant.

While the present results for the n-alkanes are listed in tables A.2 to A.5 with their respective standard uncertainties $u_{\mu_{\mathrm{fluid}}}$ and $u_{\mu_{\mathrm{b}}}$, additional results obtained with the original setup for water, toluene, 1-propanol and 2-propanol are disclosed elsewhere [17, p. 187 ff.].

The bulk viscosity can independently be determined by molecular dynamics (MD) simulation [43]. Such simulations are based on force fields describing the interactions between molecules. In the present work, the repulsive and dispersive intermolecular interactions of methanol are described by a Lennard-Jones type potential [44] and the bulk viscosity is determined on the basis of the Green-Kubo formalism [45, 46]. The latter requires the evaluation of an improper time

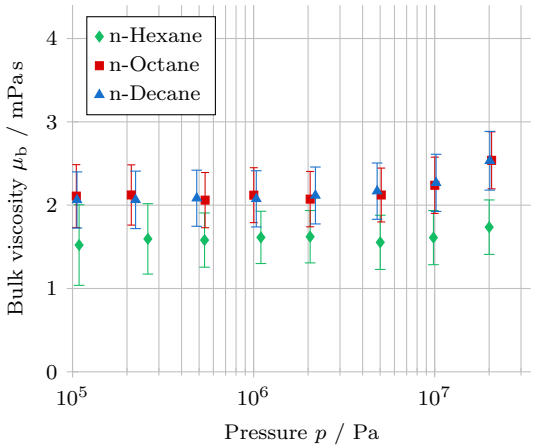

Figure 15: Bulk viscosity and its standard uncertainty of n-hexane, n-octane and n-decane at constant temperature 303 K and varying pressure.

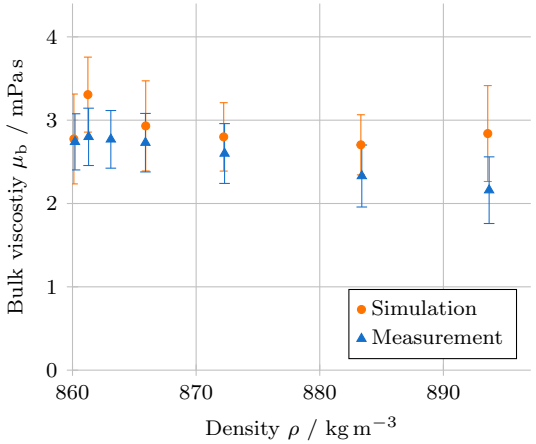

Figure 16: Comparison of bulk viscosity data for liquid methanol at constant temperature 220 K, obtained experimentally and by molecular dynamics simulation.

integral of autocorrelation functions of the stress tensor's diagonal elements [47]

$$\mu_\mathrm{b} = \frac{V}{k_\mathrm{B}T} \lim_{n\to\infty} \int_0^n \langle \delta P(0) \delta P(t) \rangle \mathrm{d}\, t \;, \tag{24}$$

with V being the volume, k_B Boltzmann's constant, $P(t)$ the instantaneous pressure, i.e. the average of the stress tensor's diagonal elements, and $P(0)$ the ensemble average pressure. Equation (24) is evaluated in the micro-canonical (NVE) ensemble and the necessary Hamiltonian, constituting the total energy of the molecular ensemble, is sampled in preceding canonical ensemble (NVT) simulations. Each simulation is conducted in a cubic volume with periodic boundaries containing $N = 4000$ molecules at constant temperature $T = 220.4\,\mathrm{K}$ and varying pressure, ranging from $p = 0.101\,\mathrm{MPa}$ to $60.89\,\mathrm{MPa}$. The interactions are explicitly evaluated up to a cut-off radius of 20 Å and analytic long-range corrections are employed. In order to adequately resolve the intrinsic small scale dynamics and also the slowly decaying pressure fluctuations [48], a sufficiently small integrator time step of 0.7 fs was chosen and the respective autocorrelation functions are integrated over a period of 100 ps.

In order to demonstrate the capability of the present methods to minimise the systematic measurement deviation, the bulk viscosity is first determined by acoustic absorption measurements and then compared to predictions made by molecular dynamics simulation. The results for liquid methanol at constant temperature 220 K and varying pressure are given in figure 16 and show a good overall agreement.

7. Conclusions

A measurement procedure based on the pulse-echo technique is proposed for the determination of the acoustic absorption and consequently the bulk viscosity of pure liquids over a wide range of thermodynamic states. Systematic measurement deviations that are present in the raw measurement data and depend on the properties of the fluid are reduced twofoldedly. First, modifications of the measuring cell are made and, second, signal processing in combination with a correction approach for systematic deviations based on reference data is introduced. The proposed methodology not only allows to re-investigate fluids like methanol and n-hexane at different thermodynamic states, it also allows to study previously unexplored substances, such as n-octane and n-decane.

It is the focus of ongoing research to further reduce the measurement deviation observed in the raw measurement data and to significantly decrease the measurement uncertainty. Noise levels are generally low due to the shielding by the pressure vessel, thus applying higher frequency and larger bandwidth signals seems promising, since it would increase the measurement effect in comparison with the interferences, and can straightforwardly be realised by choosing ceramic piezoelectric transducers instead of quartz. The current measurement range is limited by a lack of reference data, which in the medium term can also be generated by molecular dynamics simulation. The necessity of reference

measurements will still impose hard limits to the properties of the fluids that can be analysed, thus, the long-term goal is to create a measurement system that shows negligible systematic deviation.

Acknowledgements

The authors would like to thank the staff at *Paderborn Center for Parallel Computing* (PC^2) for providing computing resources.

Appendix A. Results and uncertainties

The standard uncertainties of the temperature and pressure measurements are 29 mK and 207 kPa, respectively [10].

Table A.2: Thermo-viscous loss μ_{fluid} and bulk viscosity μ_{b} of methanol.

T K	p MPa	μ_{fluid} mPa s	$u_{\mu_{\mathrm{fluid}}}$ mPa s	μ_{b} mPa s	$u_{\mu_{\mathrm{b}}}$ mPa s
278.3	0.1	2.15	0.34	1.14	0.34
278.3	0.2	1.88	0.36	0.87	0.33
278.3	0.6	1.98	0.32	0.97	0.32
278.3	1.1	2.13	0.32	1.12	0.32
278.3	2.2	2.19	0.32	1.17	0.32
278.3	4.9	2.09	0.32	1.05	0.32
278.3	10.0	2.49	0.32	1.42	0.32
293.3	0.1	1.69	0.44	0.89	0.35
293.3	0.3	1.62	0.35	0.83	0.32
293.3	0.6	1.85	0.32	1.05	0.32
293.3	1.1	1.78	0.31	0.98	0.31
293.3	2.0	1.58	0.31	0.78	0.32
293.3	5.2	2.09	0.31	1.27	0.32
293.3	10.2	1.77	0.31	0.93	0.32
303.2	0.1	1.66	0.49	0.97	0.38
303.2	0.2	1.66	0.40	0.97	0.35
303.2	0.7	1.66	0.32	0.97	0.31
303.2	1.1	1.54	0.31	0.84	0.31
303.2	2.1	1.66	0.31	0.96	0.31
303.2	5.0	1.54	0.31	0.82	0.31
303.2	10.1	1.68	0.31	0.95	0.31
323.2	0.1	1.49	0.60	0.96	0.46
323.2	0.2	1.50	0.52	0.97	0.41
323.2	0.5	1.54	0.34	1.00	0.33
323.2	1.1	1.48	0.31	0.95	0.31
323.2	2.3	1.47	0.31	0.93	0.31
323.2	5.2	1.64	0.31	1.09	0.31
323.2	10.5	1.59	0.31	1.03	0.32

Table A.3: Thermo-viscous loss μ_{fluid} and bulk viscosity μ_{b} of n-hexane.

T K	p MPa	μ_{fluid} mPa s	$u_{\mu_{\mathrm{fluid}}}$ mPa s	μ_{b} mPa s	$u_{\mu_{\mathrm{b}}}$ mPa s
278.3	0.1	2.61	0.48	2.10	0.44
278.3	0.2	2.62	0.43	2.11	0.39
278.3	0.5	2.70	0.33	2.18	0.33
278.3	1.2	2.63	0.33	2.12	0.33
278.3	2.1	2.66	0.33	2.14	0.33
278.3	5.1	2.74	0.33	2.19	0.33
278.3	9.9	2.89	0.34	2.31	0.34
278.3	19.7	3.33	0.34	2.68	0.34
293.3	0.1	2.17	0.53	1.74	0.47
293.3	0.2	2.13	0.44	1.69	0.40
293.3	0.5	2.11	0.33	1.68	0.33
293.3	0.8	2.19	0.32	1.75	0.32
293.3	2.0	2.17	0.32	1.72	0.32
293.3	5.3	2.18	0.32	1.71	0.32
293.3	10.5	2.25	0.32	1.75	0.32
293.3	21.0	2.54	0.33	1.98	0.33
303.2	0.1	1.91	0.56	1.52	0.49
303.2	0.3	1.99	0.45	1.60	0.41
303.2	0.5	1.97	0.34	1.58	0.33
303.2	1.1	2.01	0.32	1.61	0.32
303.2	2.1	2.02	0.32	1.62	0.32
303.2	5.0	1.97	0.32	1.55	0.32
303.2	9.9	2.06	0.32	1.61	0.32
303.2	20.0	2.24	0.32	1.74	0.32
323.2	9.9	1.81	0.32	1.44	0.32
323.2	20.1	1.94	0.32	1.52	0.32

Table A.4: Thermo-viscous loss μ_{fluid} and bulk viscosity μ_{b} of n-octane.

T K	p MPa	μ_{fluid} mPa s	$u_{\mu_{\mathrm{fluid}}}$ mPa s	μ_{b} mPa s	$u_{\mu_{\mathrm{b}}}$ mPa s
278.3	0.1	3.70	0.36	2.81	0.36
278.3	0.2	3.72	0.36	2.82	0.36
278.3	0.5	3.69	0.35	2.79	0.35
278.3	1.0	3.80	0.35	2.90	0.35
278.3	2.2	3.74	0.35	2.83	0.35
278.3	5.0	3.84	0.35	2.90	0.35
278.3	10.2	4.10	0.36	3.10	0.36
278.3	20.1	4.58	0.37	3.48	0.37
293.3	0.1	3.00	0.37	2.27	0.35
293.3	0.2	3.06	0.37	2.32	0.36
293.3	0.5	3.00	0.33	2.27	0.33
293.2	0.9	2.95	0.33	2.21	0.33
293.3	2.1	2.99	0.34	2.24	0.34
293.3	4.8	3.06	0.34	2.29	0.34
293.3	10.2	3.41	0.34	2.60	0.34
293.3	21.1	3.75	0.35	2.84	0.35
303.2	0.1	2.76	0.42	2.11	0.37
303.2	0.2	2.78	0.37	2.12	0.35
303.2	0.5	2.72	0.33	2.06	0.33
303.2	1.0	2.78	0.33	2.12	0.33
303.2	2.1	2.74	0.33	2.07	0.33
303.2	5.1	2.81	0.33	2.12	0.33
303.2	10.0	2.96	0.33	2.24	0.33
303.2	20.6	3.34	0.35	2.54	0.35
323.2	0.1	2.30	0.45	1.77	0.40
323.2	0.2	2.27	0.31	1.74	0.36
323.2	0.5	2.32	0.33	1.79	0.33
323.2	1.0	2.28	0.32	1.75	0.32
323.2	2.0	2.31	0.33	1.77	0.33
323.2	5.3	2.42	0.33	1.87	0.33
323.2	10.2	2.51	0.33	1.92	0.33
323.2	20.7	2.68	0.33	2.03	0.33
349.9	10.2	2.11	0.32	1.66	0.32
349.9	20.3	2.29	0.32	1.78	0.32

Table A.5: Thermo-viscous loss μ_{fluid} and bulk viscosity μ_{b} of n-decane.

T K	p MPa	μ_{fluid} mPa s	$u_{\mu_{\mathrm{fluid}}}$ mPa s	μ_{b} mPa s	$u_{\mu_{\mathrm{b}}}$ mPa s
278.3	0.1	4.76	0.38	3.19	0.38
278.3	0.2	4.75	0.37	3.18	0.37
278.3	0.5	4.72	0.37	3.15	0.37
278.3	1.1	4.84	0.38	3.25	0.38
278.3	2.0	4.86	0.38	3.26	0.38
278.3	4.9	5.10	0.38	3.44	0.38
278.3	10.0	5.28	0.39	3.52	0.39
278.3	20.0	5.94	0.41	3.98	0.41
293.2	0.1	3.71	0.36	2.48	0.36
293.2	0.3	3.74	0.35	2.50	0.35
293.2	0.5	3.71	0.35	2.48	0.35
293.2	1.0	3.77	0.35	2.52	0.35
293.2	2.0	3.76	0.35	2.50	0.35
293.2	5.2	3.91	0.35	2.60	0.35
293.2	10.1	4.20	0.36	2.82	0.36
293.2	20.5	4.61	0.37	3.07	0.37
303.2	0.1	3.13	0.35	2.06	0.34
303.2	0.2	3.13	0.34	2.06	0.34
303.2	0.5	3.15	0.34	2.08	0.34
303.2	1.0	3.15	0.34	2.08	0.34
303.2	2.2	3.21	0.34	2.12	0.34
303.2	4.8	3.29	0.34	2.17	0.34
303.2	10.2	3.46	0.35	2.27	0.35
303.2	20.2	3.86	0.36	2.53	0.36
323.2	0.1	2.55	0.35	1.72	0.34
323.2	0.2	2.57	0.34	1.75	0.33
323.2	0.5	2.57	0.33	1.74	0.33
323.2	1.0	2.52	0.33	1.69	0.33
323.2	2.0	2.61	0.33	1.77	0.33
323.2	5.2	2.65	0.33	1.77	0.33
323.2	10.0	2.70	0.33	1.77	0.33
323.2	20.2	2.96	0.33	1.93	0.33
350.0	0.1	1.91	0.37	1.29	0.34
350.0	0.2	1.94	0.34	1.32	0.33
350.0	0.5	1.92	0.32	1.30	0.32
350.0	1.1	2.01	0.32	1.38	0.32
350.0	2.1	1.96	0.32	1.33	0.32
350.0	5.0	2.00	0.32	1.35	0.32
350.0	9.9	2.18	0.32	1.49	0.32
350.0	20.0	2.28	0.32	1.51	0.32
361.1	2.1	1.70	0.31	1.14	0.31
361.1	4.8	1.75	0.32	1.16	0.32
361.1	9.8	1.86	0.32	1.24	0.32
361.1	20.0	2.11	0.32	1.42	0.32

References

References

[1] L. D. Landau, E. M. Lifshitz, Fluid mechanics, Pergamon Press, Oxford, England, 1987.

[2] A. Chikitkin, B. Rogov, G. Tirsky, S. Utyuzhnikov, Effect of bulk viscosity in supersonic flow past spacecraft, Applied Numerical Mathematics 93 (2015) 47–60. doi:10.1016/j.apnum.2014.01.004.

[3] G. Emanuel, Effect of bulk viscosity on a hypersonic boundary layer, Physics of Fluids A: Fluid Dynamics 4 (3) (1992) 491–495. doi:10.1063/1.858322.

[4] H. Weyl, Shock waves in arbitrary fluids, Communications on Pure and Applied Mathematics 2 (2-3) (1949) 103–122. doi:10.1002/cpa.3160020201.

[5] D. Gilbarg, D. Paolucci, The structure of shock waves in the continuum theory of fluids, Journal of Rational Mechanics and Analysis 2 (1953) 617–642. doi:10.1512/iumj.1953.2.52031.

[6] H. A. Bethe, On the Theory of Shock Waves for an Arbitrary Equation of State, Springer, New York, 1998, pp. 421–495. doi:10.1007/978-1-4612-2218-7_11.

[7] F. Bahmani, M. Cramer, Suppression of shock-induced separation in fluids having large bulk viscosities, Journal of Fluid Mechanics 756 (2014) R2. doi:10.1017/jfm.2014.494.

[8] O. V. Rudenko, S. I. Solujan, R. T. Beyer, Theoretical foundations of nonlinear acoustics, Studies in Soviet science, Consultants Bureau, New York, 1977.

[9] M. J. Buckingham, Causality, Stokes' wave equation, and acoustic pulse propagation in a viscous fluid, Physical Review E 72 (2) (8 2005). doi:10.1103/PhysRevE.72.026610.

[10] F. H. Dubberke, D. B. Rasche, E. Baumhögger, J. Vrabec, Apparatus for the measurement of the speed of sound of ammonia up to high temperatures and pressures, Review of Scientific Instruments 85 (8) (2014) 084901. doi:10.1063/1.4891795.

[11] J. M. M. Pinkerton, A Pulse Method for the Measurement of Ultrasonic Absorption in Liquids: Results for Water, Nature 160 (1947) 128–129. doi:10.1038/160128b0.

[12] T. A. Litovitz, E. H. Carnevale, Effect of Pressure on Sound Propagation in Water, Journal of Applied Physics 26 (7) (1955) 816–820. doi:10.1063/1.1722101.

[13] W. H. Johnson Jr., G. Holton, Analysis of Ultrasonic Absorption Measurements in Liquids at High Pressure, Review of Scientific Instruments 39 (9) (1968) 1247–1253. doi:10.1063/1.1683643.

[14] M. Holmes, N. Parker, M. Povey, Temperature dependence of bulk viscosity in water using acoustic spectroscopy, Journal of Physics: Conference Series 269 (1) (2011) 012011. doi:10.1088/1742-6596/269/1/012011.

[15] M. A. Javed, E. Baumhögger, J. Vrabec, Thermodynamic Speed of Sound Data for Liquid and Supercritical Alcohols, Journal of Chemical & Engineering Data 64 (3) (2019) 1035–1044. doi:10.1021/acs.jced.8b00938.

[16] E. H. Carnevale, T. A. Litovitz, Pressure Dependence of Sound Propagation in the Primary Alcohols, The Journal of the Acoustical Society of America 27 (3) (1955) 547–550. doi:10.1121/1.1907959.

[17] L. Claes, Messverfahren für die akustische Absorption in reinen Fluiden zur Bestimmung der Volumenviskosität (measurement procedure for acoustic absorption in pure fluids to determine bulk viscosity), Ph.D. thesis (2021). doi:10.17619/UNIPB/1-1104.

[18] M. Fink, F. Hottier, J. F. Cardoso, Ultrasonic Signal Processing for in Vivo Attenuation Measurement: Short Time Fourier Analysis, Ultrasonic Imaging 5 (2) (1983) 117–135. doi:10.1177/016173468300500202.

[19] Y. Quan, J. M. Harris, Seismic attenuation tomography using the frequency shift method, GEOPHYSICS 62 (3) (1997) 895–905. doi:10.1190/1.1444197.

[20] L. Claes, R. S. Chatwell, J. Vrabec, B. Henning, A Spectral Approach to Acoustic Absorption Measurement, in: AMA Service GmbH (Ed.), PROCEEDINGS – AMA Conferences 2017, 2017, pp. 304–309. doi:10.5162/sensor2017/C1.2.

[21] L. Claes, S. Johannesmann, E. Baumhögger, B. Henning, Quantification of frequency-dependent absorption phenomena, in: Proceedings of Meetings on Acoustics, Vol. 38, ASA, 2019, p. 055002. doi:10.1121/2.0001043.

[22] L. Claes, M. Webersen, pyfds 0.1.3 – modular field simulation tool, github.com/emtpb/pyfds (3 2020). doi:10.5281/zenodo.3706625.

[23] L. Claes, H. Zeipert, P. Koppa, T. Tröster, B. Henning, Additively manufactured acoustic diffuser structures for ultrasonic measurement applications, in: Proceedings of Meetings on Acoustics, Vol. 32, ASA, 2018, p. 030004. doi:10.1121/2.0000688.

[24] S. A. Hawley, J. R. Allegra, G. Holton, Ultrasonic-Absorption and Sound-Speed Data for Nine Liquids at High Pressures, The Journal of the Acoustical Society of America 47 (1B) (1970) 137–143. doi:10.1121/1.1911444.

[25] S. K. Kor, O. N. Awasthi, G. Rai, S. C. Deorani, Structural Absorption of Ultrasonic Waves in Methanol, Physical Review A 3 (1) (1971) 390–393. doi:10.1103/physreva.3.390.

[26] L. Claes, L. M. Hülskämper, E. Baumhögger, N. Feldmann, R. S. Chatwell, J. Vrabec, B. Henning, Acoustic absorption measurement for the determination of the volume viscosity of pure fluids, tm - Technisches Messen 86 (s1) (2019) 2–6. doi:10.1515/teme-2019-0038.

[27] H. W. Xiang, A. Laesecke, M. L. Huber, A new reference correlation for the viscosity of methanol, Journal of physical and chemical reference data 35 (4) (2006) 1597–1620. doi:10.1063/1.2360605.

[28] E. K. Michailidou, M. J. Assael, M. L. Huber, R. A. Perkins, Reference Correlation of the Viscosity of n-Hexane from the Triple Point to 600 K and up to 100 MPa, Journal of Physical and Chemical Reference Data 42 (3) (2013) 033104. doi:10.1063/1.4818980.

[29] E. A. Sykioti, M. J. Assael, M. L. Huber, R. A. Perkins, Reference Correlation of the Thermal Conductivity of Methanol from the Triple Point to 660 K and up to 245 MPa, Journal of Physical and Chemical Reference Data 42 (4) (2013) 043101. doi:10.1063/1.4829449.

[30] M. J. Assael, S. K. Mylona, C. A. Tsiglifisi, M. L. Huber, R. A. Perkins, Reference Correlation of the Thermal Conductivity of n-Hexane from the Triple Point to 600 K and up to 500 MPa, Journal of Physical and Chemical Reference Data 42 (1) (2013) 013106. doi:10.1063/1.4793335.

[31] L. Piazza, R. Span, An equation of state for methanol including the association term of SAFT, Fluid Phase Equilibria 349 (2013) 12–24. doi:10.1016/j.fluid.2013.03.024.

[32] R. Span, W. Wagner, Equations of State for Technical Applications. II. Results for Nonpolar Fluids, International Journal of Thermophysics 24 (1) (2003) 41–109. doi:10.1023/a:1022310214958.

[33] J. R. Allegra, S. A. Hawley, G. Holton, Pressure Dependence of the Ultrasonic Absorption in Toluene and Hexane, The Journal of the Acoustical Society of America 47 (1B) (1970) 144–150. doi:10.1121/1.1911446.

[34] S. K. Kor, S. C. Deorani, B. K. Singh, Origin of Ultrasonic Absorption in Methanol, Physical Review A 3 (5) (1971) 1780–1783. doi:10.1103/PhysRevA.3.1780.

[35] O. Awasthi, Temperature dependence of ultrasonic attenuation in associated liquids, Physics Letters A 61 (2) (1977) 122–124. doi:10.1016/0375-9601(77)90857-x.

[36] C. B. Barber, D. P. Dobkin, H. Huhdanpaa, The Quickhull algorithm for convex hulls, ACM Transactions on Mathematical Software 22 (4) (1996) 469–483. doi:10.1145/235815.235821.

[37] M. Cox, P. Harris, B. R.-L. Siebert, Evaluation of Measurement Uncertainty Based on the Propagation of Distributions Using Monte Carlo Simulation, Measurement Techniques 46 (9) (2003) 824–833. doi:10.1023/b:mete.0000008439.82231.ad.

[38] Joint Committee for Guides in Metrology, Guide to the Expression of Uncertainty in Measurement (2008).

[39] DAkkS, Bestimmung von Thermometerkennlinien (determination of the characteristic curve of thermometers), Tech. rep., Deutsche Akkreditierungsstelle GmbH (2010).

[40] M. L. Huber, A. Laesecke, H. W. Xiang, Viscosity correlations for minor constituent fluids in natural gas: n-octane, n-nonane and n-decane, Fluid Phase Equilibria 228-229 (2005) 401–408. doi:10.1016/j.fluid.2005.03.008.

[41] M. Huber, R. Perkins, Thermal conductivity correlations for minor constituent fluids in natural gas: n-octane, n-nonane and n-decane, Fluid Phase Equilibria 227 (1) (2005) 47–55. doi:10.1016/j.fluid.2004.10.031.

[42] E. W. Lemmon, R. Span, Short Fundamental Equations of State for 20 Industrial Fluids, Journal of Chemical & Engineering Data 51 (3) (2006) 785–850. doi:10.1021/je050186n.

[43] R. S. Chatwell, J. Vrabec, Bulk viscosity of liquid noble gases, The Journal of Chemical Physics 152 (9) (2020) 094503. doi:10.1063/1.5142364.

[44] T. Schnabel, A. Srivastava, J. Vrabec, H. Hasse, Hydrogen bonding of methanol in supercritical CO_2: Comparison between 1H NMR spectrocopic data and molecular simulation results, The Journal of Physical Chemistry B 111 (33) (2007) 9871–9878. doi:10.1021/jp0720338.

[45] R. Kubo, Statistical-mechanical theory of irreversible processes. I. General theory and simple applications to magnetic and conduction problems, Journal of the Physical Society of Japan 12 (6) (1957) 570–586. doi:10.1143/JPSJ.12.570.

[46] M. S. Green, Markoff random processes and the statistical mechanics of time-dependent phenomena II. Irreversible processes in fluids, Journal of Chemical Physics 22 (3) (1954) 398–414. doi:10.1063/1.1740082.

[47] G.-J. Guo, Y.-G. Zhang, Equilibrium molecular dynamics calculation of the bulk viscosity of liquid water, Molecular Physics 99 (4) (2001) 283–289. doi:10.1080/00268970010011762.

[48] G. S. Fanourgakis, J. S. Medina, R. Prosmiti, Determining the bulk viscosity of rigid water molecules, Journal of Physical Chemistry A 116 (10) (2012) 2564–2570. doi:10.1021/jp211952y.